Chapter 2

Residual prestack migration and velocity analysis

2.1 Introduction and overview

2.1.1 Historical background

Zero-offset migration with velocity v_2 after initial migration with v_1 gives the same result as zero-offset migration velocity with $v_m = \sqrt{v_1^2 + v_2^2}$. This migration after an initial migration is called residual migration (also called cascaded migration) (Rothman et al., 1985). Residual zero-offset migration changes the migration velocity of an already migrated zero-offset section without remigrating the data from scratch and has proven to be very useful. Larner and Beasley (1987) used residual migration to enhance the accuracy of 15 degree migrations, extending them to higher dips. Beasley et al., (1988) use cascaded migration to extend Stolt (constant velocity f–k) migration to depth-variable velocity media.

Al-Yahya and Fowler (1986) explored residual prestack migration hoping to provide a method for changing prestack migration velocities as easily as zero-offset migration velocities can be changed with residual zero-offset migration. This might make it possible to depth-migrate data before stack by first applying an inexpensive prestack time migration followed by residual prestack migration to account for the lateral velocity variation. They concluded that it is possible to construct an operator that converts constant-offset

or shot-profile data, migrated with one velocity, to an image migrated at another velocity; but unlike residual zero-offset migration, the operator is not equivalent to applying prestack migration with some other velocity. Because the operator they obtained was not a conventional "migration," it seemed that residual prestack migration would not be so useful as residual zero-offset migration.

2.1.2 Residual prestack migration for velocity analysis

To be efficient, velocity analysis after prestack depth migration should find the effect of a change in interval velocity on migrated images without remigrating from scratch. It is also important to use the guidelines of section 1.3 to build a velocity-analysis method for prestack depth migration. This chapter formulates residual prestack migration and shows how it can be used as a velocity-analysis tool. The formulation for residual prestack migration described in this chapter uses migrated constant-offset sections, but residual prestack migration can be defined for migrated shot profiles as well (Zhang, 1990).

Residual time or depth migration?

Residual migration can be formulated as a depth migration or a time migration. Residual time migration like conventional time migration requires specification of one parameter, the residual velocity. Residual depth migration, like conventional depth migration, requires specification of an interval-velocity model. Residual depth migration gives more accurate images than residual time migration because by definition, residual depth migration honors the ray-bending implied both by the initial velocity model and the updated interval-velocity model. Residual time migration uses reflector movement derived with constant-velocity assumptions, so residual time migration only honors the ray-bending due to the initial velocity model if the initial migration is a depth migration. Although residual time migration does not position images as accurately as residual depth migration, residual time migration is often adequate, especially when a small amount of residual migration is needed.

The greatest drawback of residual depth migration is the need to specify an interval-velocity model. This makes velocity analysis with residual prestack depth migration nearly as difficult as velocity analysis based on prestack depth migration alone. Residual prestack time migration allows one to build a velocity-analysis cube of all possible residual prestack time migrations, a powerful velocity-analysis tool. In Chapter 3 I show how to build an

approximate residual depth migration for small changes to the interval-velocity model by appropriately selecting images from the space of all residual time migrations. For the purposes of this thesis, residual prestack migration is a velocity-analysis tool and is more appropriate cast as a time migration. When accurate imaging is required after substantially changing the interval-velocity model, I will depth-migrate the data from scratch with the new model.

Although for the rest of this chapter I only discuss residual prestack time migration, the principles for deriving residual prestack depth migration are the same as those for residual prestack time migration. Analytical methods can't be used to find the kinematics of a residual prestack depth-migration operator, so extensive ray-tracing or other traveltime computations (Vidale, 1988; Van Trier and Symes, 1990) are necessary.

Excluding zero-offset migration

By analogy to conventional prestack time migration (Hale, 1983), the kinematics of residual prestack time migration can be separated into three parts: residual NMO, residual DMO, and residual zero-offset migration. As discussed in the introduction, the moveout and common-reflection-point gathering necessary for proper migration velocity analysis are controlled only by residual NMO and residual DMO. The zero-offset residual-migration component is the same for all offsets and does not affect how well the same events on different migrated constant-offset sections stack together, but it confuses velocity analysis by moving events as residual velocity changes.

It is preferable to focus attention on individual events and study them at a fixed location as residual velocity changes. Section 2.3 shows how to remove the zero-offset residual-migration component of residual prestack migration leaving residual NMO+DMO. Later, in Chapter 3, the zero-offset residual-migration component of residual prestack migration will turn out to be a necessary part of tomographic inversion for interval velocities. Although residual zero-offset migration is not applied to the data when scanning residual velocity, I keep track of its kinematics.

2.2 Residual constant-offset migration

2.2.1 Definition

Define residual constant-offset migration as the process that converts a constant-offset section migrated with velocity v to a constant-offset section migrated with velocity v_n. We can get that operator by cascading two processes: constant-offset modeling with velocity v which "undoes" the first migration, followed by constant-offset migration with velocity v_n.

Constant-offset modeling is represented by the Kirchhoff-integral operator

$$D(\omega,\xi) = \int_{\mathbf{X}} A(\xi,h,\mathbf{x},\omega)\; R(\mathbf{x})\; e^{i\varphi(\xi,h,\mathbf{x},\omega,v)}\; d\mathbf{x}\;. \tag{2.1}$$

In equation (2.1), $R(\mathbf{x})$ is the input image of the reflectivity of the subsurface; $D(\omega,\xi)$ is the output data as a function of temporal frequency ω, midpoint ξ, and offset h. $A(\xi,h,\mathbf{x},\omega,v)$ is the amplitude of the integral operator; $\varphi(\xi,h,\mathbf{x},\omega,v)$ is the phase of the integral operator which is controlled by the traveltime of waves from the source to reflector to receiver. The phase function φ and amplitude function A are discussed by Bleistein (1986) and Deregowski and Brown (1983) and also described in more detail in Appendix A. Constant-offset migration (Deregowski, 1985; LeBras and Clayton, 1988) is given by the integral operator

$$R'(\mathbf{x}') = \int_{\xi}\int_{\omega} B(\xi,h,\mathbf{x}',\omega)\; D(\omega,\xi)\; e^{-i\varphi(\xi,h,\mathbf{x}',\omega,v)}\; d\xi\; d\omega\;; \tag{2.2}$$

where $R'(\mathbf{x}')$ is the new output reflectivity. Residual constant-offset migration is formally obtained by rewriting the two processes represented by equations (2.1) and (2.2) as a single process.

$$\begin{aligned} R'(\mathbf{x}') \;=\; & \int_{\xi}\int_{\omega}\int_{\mathbf{X}} A(\xi,h,\mathbf{x}',\omega)B(\xi,h,\mathbf{x}',\omega) \\ & e^{i[\varphi(\xi,h,\mathbf{x},\omega,v)-\varphi(\xi,h,\mathbf{x}',\omega,v_n)]}\; R(\mathbf{x})\; d\mathbf{x}\; d\xi\; d\omega\;. \end{aligned} \tag{2.3}$$

Applying residual constant-offset migration using equation (2.3) offers no advantage over just migrating the original data with the new velocity. It is twice as expensive since it implies we have to model the data then remigrate it.

2.2.2 Asymptotic residual constant-offset migration

Most seismic reflection data are collected in the far-field; the reflected waves of interest to us travel several wavelengths between source and reflectors and between reflectors and receivers. Furthermore, the most important property of residual prestack migration for velocity analysis is the kinematic repositioning of reflector images. Both of these facts suggest simplified evaluation of the integrals in equation (2.3) using asymptotic techniques. Rewrite equation (2.3) changing the order of integration.

$$R'(\mathbf{x}') = \int_{\mathbf{X}} \int_{\omega} \int_{\xi} A(\xi, h, \mathbf{x}', \omega) B(\xi, h, \mathbf{x}', \omega) \\ e^{i[\varphi(\xi,h,\mathbf{x},\omega,v) - \varphi(\xi,h,\mathbf{x}',\omega,v_n)]} \, R(\mathbf{x}) \, d\xi \, d\omega \, d\mathbf{x} \; . \tag{2.4}$$

In Appendix B, I show how to evaluate asymptotically the integrals over ξ using the method of stationary phase and how to evaluate the integrals over ω by inverting a Fourier transform. After these evaluations, a one-dimensional integral over a curvilinear path remains. This integration path describes the kinematics of the residual-migration operator, the most important part of the operator for velocity analysis. I merely quote the result here in compact form since the expressions are lengthy and their exact form is immaterial at this point. See Appendix B for detailed expressions of the factors in equation (2.5)

$$R'(\mathbf{x}') = \int_{X_s} K(\mathbf{x}', \mathbf{x}_s) \; D_{\pm t}^{\frac{1}{2}} \; R(\mathbf{x}_s) \; d\mathbf{x}_s \; . \tag{2.5}$$

The important thing to notice about equation (2.5) is that it has a form similar to the equation for constant-offset migration; it is another integral operator. Instead of integrating over data traces in time and midpoint, it integrates over a trajectory through the initial migrated image. The domain of integration X_s for a single $\mathbf{x}'$ is the one-dimensional trajectory in $\mathbf{x}$ that describes the kinematics of the operator. I describe how to find this trajectory in the next section. $D_{\pm t}^{\frac{1}{2}}$ is a convolutional operator that arises from the stationary phase approximation and the inverse transform over ω. The convolution is a 1-D convolution in the direction of increasing time and constant time-dip in the initial image. The exponent signifies that the spectrum of the convolutional operator is the same as the spectrum of a derivative of one-half order. The integration weights $K(\mathbf{x}', \mathbf{x}_s)$ contain factors from the amplitudes of both modeling (equation (2.1)) and migration

(equation (2.2)) and from the stationary phase calculation (see Appendix B).

For small changes to the migration velocity, the integration trajectory can be discretized with fewer points than required to sample a conventional constant-offset migration operator for velocity v_n; applying residual constant-offset migration is less expensive than migrating the data from scratch.

2.2.3 Geometrical derivation of residual constant-offset migration

Finding how the image of a dipping reflector moves when migration velocity changes describes the kinematics of residual constant-offset migration. This geometric derivation of residual prestack migration illustrates the physical meaning of the mathematics in Appendix B and the previous section.

The impulse response of constant-velocity constant-offset migration is an ellipse with foci at source and receiver. A small segment of a dipping reflection event corresponding to a point in the data containing a single traveltime and traveltime dip becomes a tangent to the impulse-response ellipse after migration. The traveltime determines the size of the ellipse, and the traveltime dip determines the position of the image along the impulse-response ellipse. This is also true in reverse; given an offset, an image point on a reflector and its dip, we can solve for the position of the source-receiver midpoint that observes a specular reflection from the image point.

Consider a point diffractor P composed of all dips from -90 to 90 degrees at an image point (x, z). To find the residual constant-offset migration that images the point P for a change in velocity from v to v_n, find where each dipping reflector segment that comprises the point diffractor comes from as the velocity changes from v to v_n. This family of points defines the summation path of the residual-migration operator.

Given a half-offset h, point P, and one candidate dipping reflector segment, we can find the midpoint ξ, the specular ray pair that illuminates P, and the migration impulse-response ellipse that goes through P as shown in Figure 2.1. This is the image of a single reflection event in the data migrated with velocity v_n. Write the traveltime of the reflection event as (now using slowness w_n instead of velocity v_n)

$$t = w_n \left[\sqrt{(x - \xi + h)^2 + z^2} + \sqrt{(x - \xi - h)^2 + z^2} \right] \quad . \tag{2.6}$$

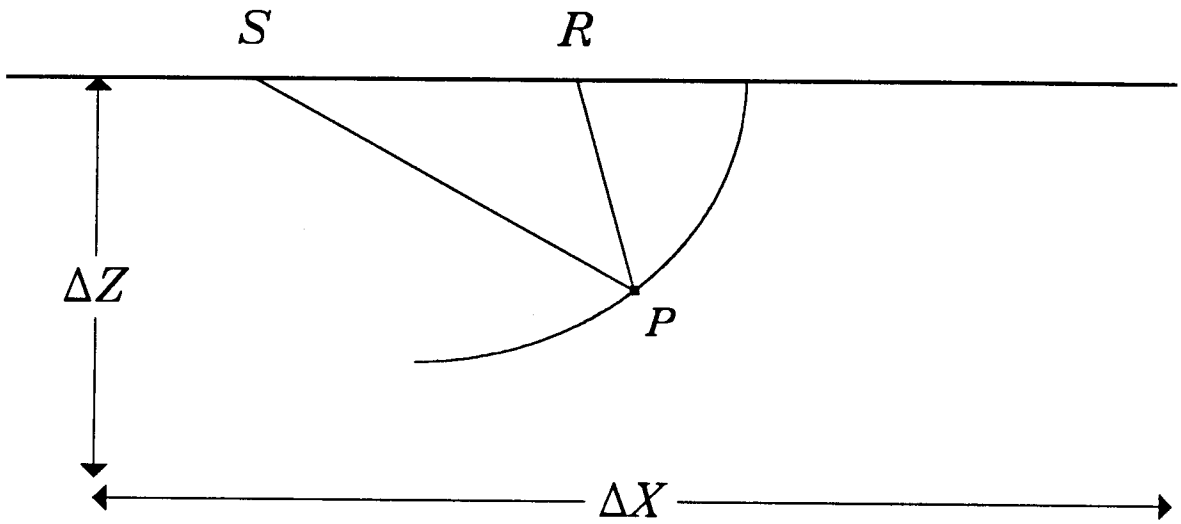

FIG. 2.1. Choosing a depth point P and a dip determines the shot-receiver pair that contains the specular reflection from the point and thus the migration impulse response that goes through P.

Also write the time dip of the event as

$$\frac{\partial t}{\partial \xi} = w_n \left[\frac{-(x-\xi+h)}{\sqrt{(x-\xi+h)^2+z^2}} + \frac{-(x-\xi-h)}{\sqrt{(x-\xi-h)^2+z^2}} \right] . \tag{2.7}$$

Changing the migration velocity changes the size of the impulse-response ellipse and the mapping from time dip to migrated dip as shown in Figure 2.2. The goal is to find point P', the image location of the reflection event of interest when the data are migrated with velocity v. The key to finding P' as the migration velocity changes is to remember that the traveltime t, midpoint ξ, and traveltime dip of the reflector segment $\partial t/\partial \xi$ are fixed because the same event in the data generates both migrated images. Only the migrated image changes as the migration slowness changes. These two conditions are the same as the stationarity condition in ξ and of non-zero contribution to the inverse transform of the integral in ω from the previous section and Appendix B.

Conserving traveltime and traveltime dip, rewrite equations (2.6) and (2.7) for P' at

velocity v (slowness w).

$$t = w\left[\sqrt{(x'-\xi+h)^2+z'^2}+\sqrt{(x'-\xi-h)^2+z'^2}\right] \quad . \tag{2.8}$$

$$\frac{\partial t}{\partial \xi} = w\left[\frac{-(x'-\xi+h)}{\sqrt{(x'-\xi+h)^2+z'^2}}+\frac{-(x'-\xi-h)}{\sqrt{(x'-\xi-h)^2+z'^2}}\right] \quad . \tag{2.9}$$

Equating the right-hand sides of equations (2.6) to (2.8) and (2.7) to (2.9) leads to a system of two equations and two unknowns to solve for x' and z', the location of the event using migration velocity v.

$$\begin{aligned} t &= w_n\left[\sqrt{(x-\xi+h)^2+z^2}+\sqrt{(x-\xi-h)^2+z^2}\right] \quad . \\ &= w\left[\sqrt{(x'-\xi+h)^2+z'^2}+\sqrt{(x'-\xi-h)^2+z'^2}\right] \qquad (2.10) \\ \frac{\partial t}{\partial \xi} &= w_n\left[\frac{-(x-\xi+h)}{\sqrt{(x-\xi+h)^2+z^2}}+\frac{-(x-\xi-h)}{\sqrt{(x-\xi-h)^2+z^2}}\right] \\ &= w\left[\frac{-(x'-\xi+h)}{\sqrt{(x'-\xi+h)^2+z'^2}}+\frac{-(x'-\xi-h)}{\sqrt{(x'-\xi-h)^2+z'^2}}\right] \quad . \qquad (2.11) \end{aligned}$$

As suggested by Al-Yahya (1987), substitute $\gamma = w_n/w$ in equation (2.10) and (2.11) since the kinematics depend only on the ratio of the slownesses and not the slownesses themselves. Call γ the residual slowness; it is a slowness scale factor. When $\gamma = 1$, residual migration leaves the image unchanged. Applying residual constant-offset migration with $\gamma < 1$ decreases the migration slowness of the image. Applying residual constant-offset migration with $\gamma > 1$ increases the migration slowness of the image. The definition of residual slowness presented here is different from other definitions of residual slowness but is convenient because γ is a dimensionless measure of slowness change.

Rather than solving equations (2.10) and (2.11) for x' and z', change variables to simplify the equations and solve for quantities that can be related to x' and z'. I parameterize the equations using the take-off angles of the specular rays to the reflector point. Referring to Figure 2.3 for the meanings of the new variables, the traveltime-dip equation

(equation (2.7)) can be written as

$$\frac{\partial t}{\partial \xi} = -w_n \left[\cos\alpha + \cos\beta \right] \quad . \tag{2.12}$$

Using the law of sines and addition and subtraction formulas, the traveltime equation (equation (2.6)) can be written as

$$t = 2hw_n \left[\frac{\sin\beta}{\sin\phi} + \frac{\sin\alpha}{\sin\phi} \right] \quad . \tag{2.13}$$

With these changes, rewrite the system of two equations and two unknowns (equations (2.10) and (2.11)) as

$$\begin{aligned} \gamma 2h \left[\frac{\sin\beta}{\sin\phi} + \frac{\sin\alpha}{\sin\phi} \right] &= 2h \left[\frac{\sin\beta'}{\sin\phi'} + \frac{\sin\alpha'}{\sin\phi'} \right] \ ; \\ \gamma \left[\cos\alpha + \cos\beta \right] &= \cos\alpha' + \cos\beta' \quad . \end{aligned} \tag{2.14}$$

Since the geometrical quantities associated with the output point P are fixed, write

$$\begin{aligned} d &= 2h \left[\frac{\sin\beta}{\sin\phi} + \frac{\sin\alpha}{\sin\phi} \right] ; \\ s &= \cos\beta + \cos\alpha \quad . \end{aligned} \tag{2.15}$$

d is the sum of the lengths of the rays and s is the sum of the cosines of the take-off angles of the rays. Finally, write the system of equations as

$$\begin{aligned} \gamma d \sin(\alpha' - \beta') &= 2h \left[\sin\alpha' + \sin\beta' \right] \ ; \\ \gamma s &= \cos\alpha' + \cos\beta' \quad . \end{aligned} \tag{2.16}$$

To solve these equations, use the first equation to express α' in terms of β' and solve the second equation for $\cos\beta'$. The solution for $\cos\beta'$ is

$$\cos\beta' = \frac{1}{8} \left[4\gamma s + \frac{8h}{\gamma d} + \frac{2\gamma d}{h} + \sqrt{\left(\frac{8h}{\gamma d} + \frac{2\gamma d}{h} + 4\gamma s \right)^2 - 16\left(4 + \frac{4sh}{d} - \frac{\gamma^2 sd}{h} \right)} \right] \quad . \tag{2.17}$$

Converting the solution of equation (2.17) back to Cartesian coordinates gives (x', z'), the

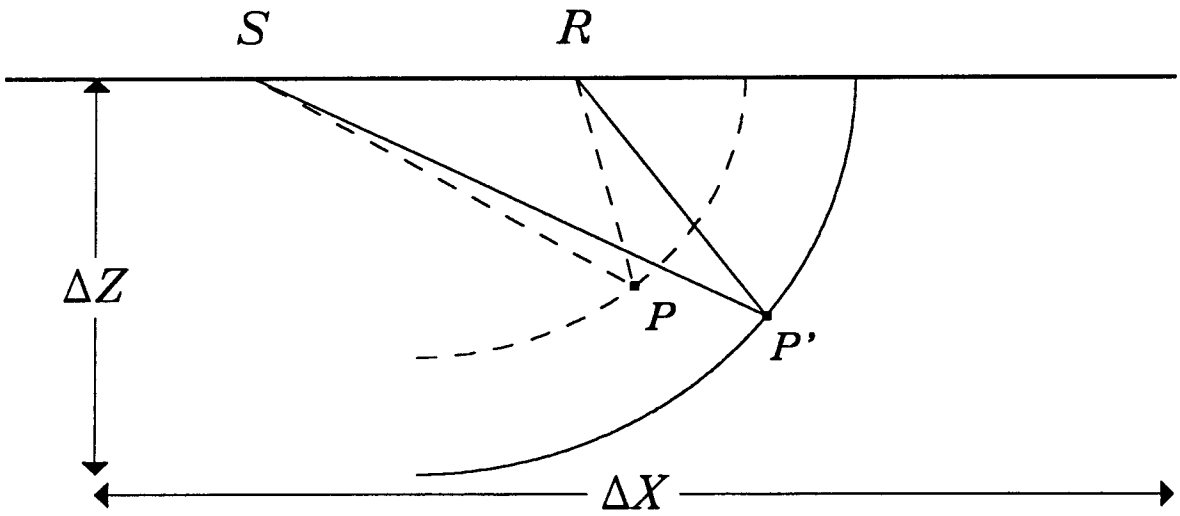

FIG. 2.2. Traveltime, traveltime dip, and midpoint are fixed, so changing the migration slowness moves the image of the reflector from input point P' to output point P.

position of the dipping reflector segment migrated with velocity v as shown in Figure 2.2.

Solving equation (2.17) for an initial point and all dips will trace out the integration path for residual constant-offset migration. Figures 2.4 and 2.5 show examples of the integration paths for residual constant-offset migration when the slowness increases or decreases respectively. Depending on the change in migration slowness and the initial depth of the reflector, these operators can have cusps. These cusps are points where the phase of the residual-migration operator has higher-order stationary points (see Appendix B) and occur only on the residual-migration operators for image points with large offset/depth ratio.

Amplitudes for discrete summation operators are obtained by computing the points on the integration paths in equal increments of the integration variables in equation (2.4) and using the stationary phase formulas from Appendix B. To prevent operator aliasing (when distance between computed points along the operator exceeds the discretization of the image), I resample the summation operators in equal arc length along the summation trajectory. The original weighting of the different parts of the operator is recovered by adjusting the amplitudes with the Jacobian of the change of variables from the original variables to arc length.

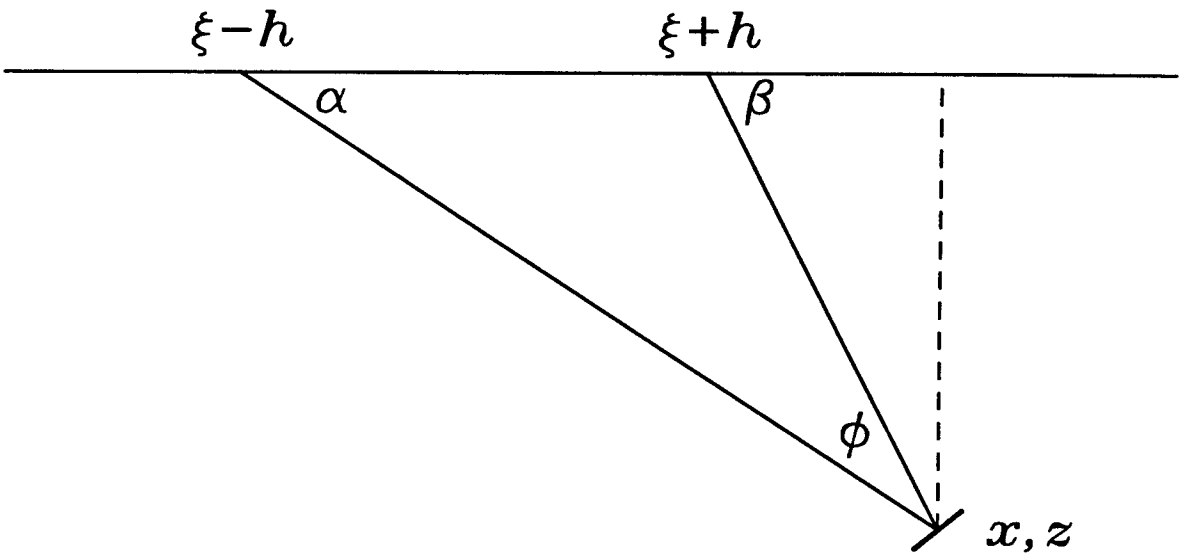

FIG. 2.3. Changing variables from Cartesian coordinates to angles of rays at the surface.

2.3 Residual NMO+DMO

Residual constant-offset migration has the desirable property that for some change in migration velocity it applies residual moveout and residual common-reflection-point gathering. After residual migration with a specified residual velocity, points with the same coordinates on two different migrated constant-offset sections correspond to the same reflection point. Residual constant-offset migration also moves all reflectors by incorporating residual zero-offset migration. If the only task is to find a residual velocity that causes the constant-offset sections to stack together coherently, the repositioning of reflectors is unnecessary and undesirable. We can exclude the repositioning of reflectors by only applying the residual moveout and residual common-reflection-point gathering part of residual constant-offset migration and omitting the part that applies residual zero-offset migration.

2.3.1 Definition

I call the operator that applies only the residual moveout and residual common-reflection-point gathering of residual prestack migration, residual NMO+DMO. To undo the zero-offset residual-migration component of residual constant-offset migration, apply residual constant-offset migration to account for the change in velocity, and follow it by residual

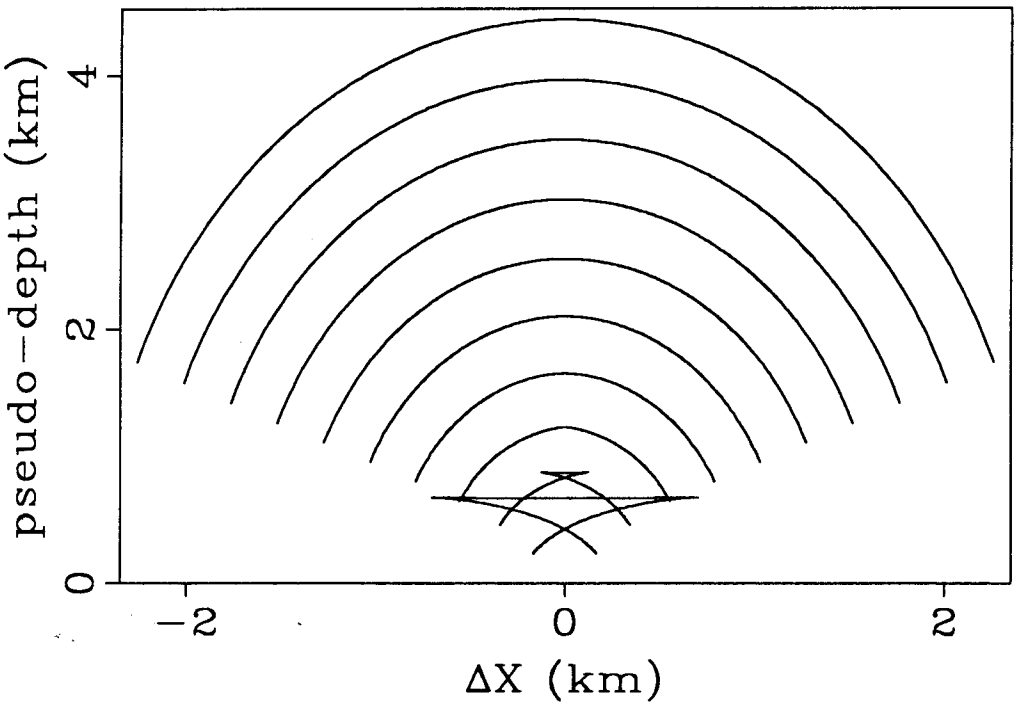

FIG. 2.4. Integration paths for residual constant-offset migration for a series of depth points. Residual slowness $\gamma = 1.2$; offset=1 km.

zero-offset modeling (residual zero-offset migration for an opposite velocity scale). This leads to a formal definition of a residual-NMO+DMO operator. The next four equations give the sequence of integral operators for applying residual constant-offset migration followed by residual zero-offset modeling.

$$D(\omega,\xi) = \int_{\mathbf{X}} A(\xi,h,\mathbf{x},\omega,v)\; R(\mathbf{x})\; e^{i\varphi(\xi,h,\mathbf{x},\omega,v)}\; d\mathbf{x} \quad . \tag{2.18}$$

$$R'(\mathbf{x}') = \int_{\xi}\int_{\omega} B(\xi,h,\mathbf{x}',\omega,v_n)\; D(\xi,\omega)\; e^{-i\varphi(\xi,h,\mathbf{x}',\omega,v_n)}\; d\xi\; d\omega \quad . \tag{2.19}$$

$$D_{zo}(\omega',\xi') = \int_{\mathbf{X}'} A(\xi',h=0,\mathbf{x}',\omega',v_n)\; R'(\mathbf{x}')\; e^{i\varphi(\xi',h=0,\mathbf{x}',\omega',v_n)}\; d\mathbf{x}' \quad . \tag{2.20}$$

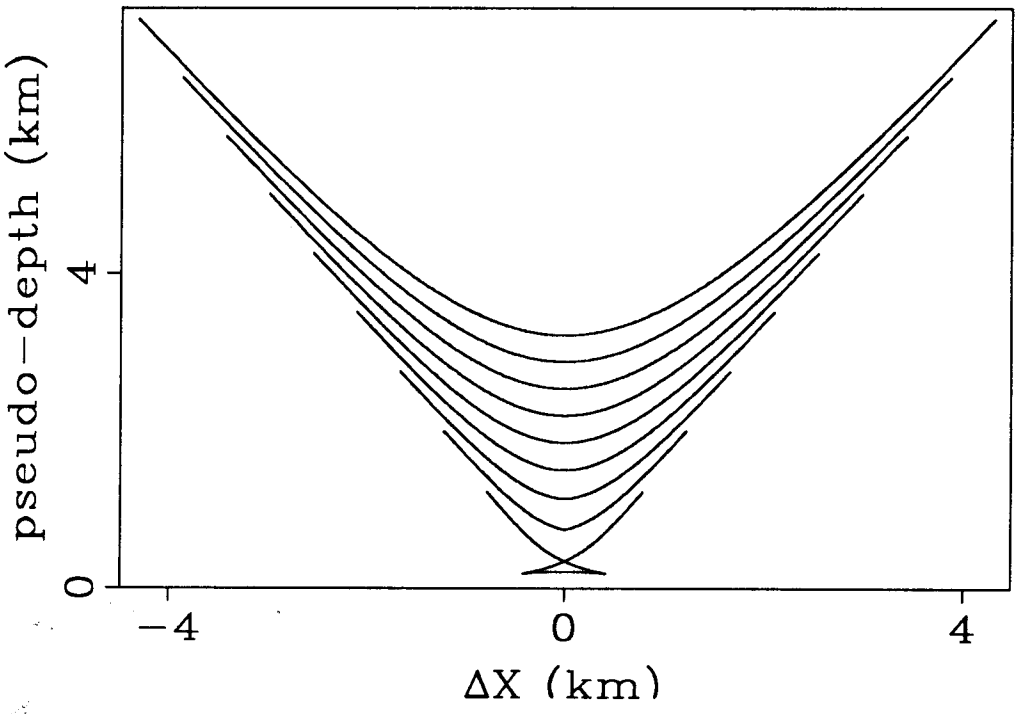

FIG. 2.5. Integration paths for residual constant-offset migration for a series of depth points. Residual slowness γ=.8; offset=1 km.

$$R''(\mathbf{x}'') = \int_{\xi'} \int_{\omega'} B(\xi', h=0, \mathbf{x}'', \omega', v)\; D_{zo}(\xi', \omega')\; e^{-i\varphi(\xi', h=0, \mathbf{x}'', \omega', v)}\; d\xi'\; d\omega' \quad . \tag{2.21}$$

As we did with residual constant-offset migration, cascade these four operators into one.

$$\begin{aligned} R''(\mathbf{x}'') \;=\; & \int_{\omega'} \int_{\xi'} \int_{\mathbf{X}'} \int_{\omega} \int_{\xi} \int_{\mathbf{X}} \Lambda(\mathbf{x}, \xi, \omega, \mathbf{x}', \xi', \omega') R(\mathbf{x}) \\ & e^{i\Psi(\mathbf{x}, \xi, \omega, \mathbf{x}', \xi', \omega')}\; d\mathbf{x}\; d\xi\; d\omega\; d\mathbf{x}'\; d\xi'\; d\omega' \quad . \end{aligned} \tag{2.22}$$

Ψ is the total phase of the operator and is the sum of the individual phases of each modeling and migration operator.

$$\begin{aligned} \Psi(\mathbf{x}, \xi, \omega, \mathbf{x}', \xi', \omega') \;=\; & \varphi(\xi, h, \mathbf{x}, \omega, v) - \varphi(\xi, h, \mathbf{x}', \omega, v_n) \\ & + \varphi(\xi', h=0, \mathbf{x}', \omega', v_n) - \varphi(\xi', h=0, \mathbf{x}'', \omega', v) \quad . \end{aligned} \tag{2.23}$$

Λ is the amplitude of the operator and is the product of the amplitudes of the individual modeling and migration operators.

$$\begin{aligned}\Lambda(\mathbf{x},\xi,\omega,\mathbf{x}',\xi',\omega',\mathbf{x}'') &= A(\xi,h,\mathbf{x},\omega,v)B(\xi,h,\mathbf{x}',\omega,v_n) \\ &\quad \times A(\xi',h=0,\mathbf{x}',\omega',v_n)B(\xi',h=0,\mathbf{x}'',\omega',v) \quad . \quad (2.24)\end{aligned}$$

2.3.2 Asymptotic residual NMO+DMO

The formal definition of residual NMO+DMO as described by equation (2.22) is too expensive to apply in practice because it requires an eight-fold integration for 2-D data; although in practice, the cost of equation (2.22) would just be the cost of four 2-D integrations. Nonetheless, as in section 2.2.2, it is desirable to simplify evaluation of residual NMO+DMO using asymptotic approximations.

The integrals that apply each residual migration can be evaluated as in the previous section. Thus, the targets for asymptotic evaluation are the integrals over ξ and ξ'. In addition one of the integrals over $\mathbf{x}'$ can be simplified asymptotically as well. The integrals over ω and ω' will be evaluated as Fourier transforms. The details of these calculations are given in Appendix B, section 2. Asymptotically evaluating the integrals over ξ, ξ', and $\mathbf{x}'$; and inverse Fourier transforming the integrals over ω and ω' leaves an integration over a one-dimensional trajectory through the original image.

$$R''(\mathbf{x}'') = \int_{\mathbf{X}_s} H(\mathbf{x}'',\mathbf{x}_s)\ \Upsilon_{t,t'}\ R(\mathbf{x}_s)\ d\mathbf{x}_s \ . \qquad (2.25)$$

Equation (2.25) is another integral operator that transforms an input constant-offset section migrated with velocity v to an output section that has been CRP-gathered and moveout corrected for velocity v_n but still displayed at the migrated location appropriate for velocity v. $R(\mathbf{x})$ is the input constant-offset section migrated with velocity v and R'' is the output section with residual NMO+DMO applied for a change of velocity to v_n. $\mathbf{X}_s$ is the integration path of residual NMO+DMO; the geometrical calculation of this summation path is detailed in the next section. $H(\mathbf{x}'',\mathbf{x}_s)$ are the appropriate weights obtained from the modeling and migration operators and from the stationary phase and Fourier transform calculations. As in equation (2.5), $\Upsilon_{t,t'}$ is a convolutional operator that takes directional derivatives of the image $R(\mathbf{x})$. Both of these factors are described in more detail in Appendix B.

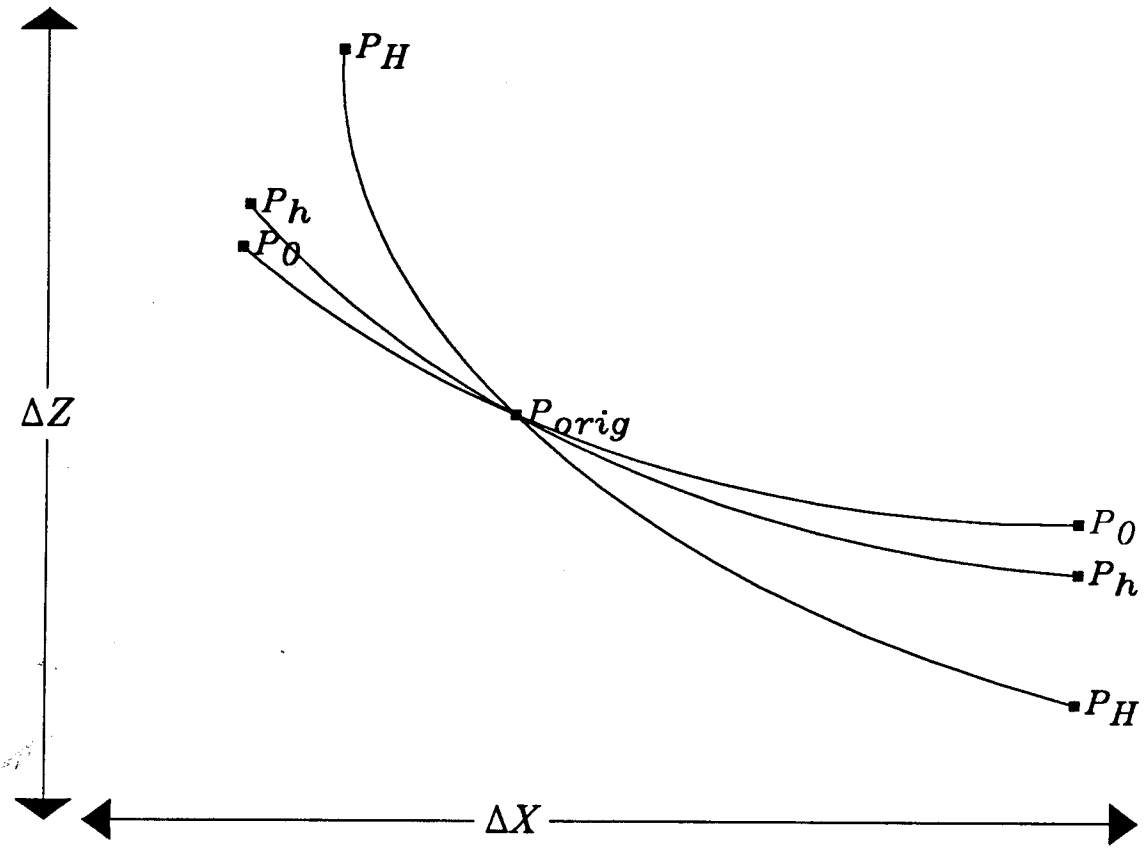

FIG. 2.6. Events on three different constant-offset sections at a fixed original point P_{orig} follow different trajectories when migration slowness changes. The top points are the positions of the image points when the slowness increases; the lower points are the positions of the image points when slowness decreases. P_0 are the positions of the zero-offset image; P_h are the positions of the image points for an offset one-half the offset of the points labeled P_H.

2.3.3 Geometrical derivation of residual NMO+DMO

Section 2.2.3 gave the necessary equations to compute the kinematics of constant-offset residual-migration operators and of zero-offset residual-migration operators by setting $h = 0$. Combining the kinematics for a residual zero-offset migration and a residual constant-offset migration for opposite velocity scales gives residual NMO+DMO. Figure 2.6 shows the positions of a point "P_{orig}" for several different values of residual slowness γ for one initial dip and 3 different offsets. The new positions P_0, P_h, and P_H for different offsets move along different trajectories as migration slowness changes. If for a fixed γ, the new

points were above one another vertically, a vertical shift, namely a residual-NMO correction, could kinematically convert constant-offset sections to zero-offset sections for a change in migration slowness. Residual constant-offset migration would be equivalent to residual NMO followed by residual zero-offset migration. For zero dip (not shown), as expected, only a vertical moveout correction and residual zero-offset migration are necessary. Residual constant-offset migration is just residual NMO followed by residual time-to-depth conversion. For non-zero dip (as shown in Figure 2.6), the points for different offsets does not belong to one CMP, kinematic conversion requires more than a vertical shift. Furthermore, the amount of the vertical movement as a function of offset is not the same as it is for zero dip. Using an analogy to full prestack migration, call residual DMO the movement required by residual constant-offset migration and not described by residual NMO or residual zero-offset migration.

Figure 2.7 shows how residual constant-offset migration can be built from three processes: residual DMO, residual NMO, and residual zero-offset migration; it graphically expresses equation (2.22). The kinematics of residual constant-offset migration image a reflector at point P_{orig} by grabbing the reflector at P_h and moving it to P_{orig}. The kinematics of residual NMO+DMO take a point P_h, move it to P_{orig} using residual constant-offset migration, then move it from P_{orig} to P_0 with residual zero-offset migration using an opposite velocity scale. Of course, we can replace this sequence of moves with the net result, the movement from P_h to P_0 following the arrows backwards along the RDMO and RNMO paths in Figure 2.7.

Figure 2.8 shows the integration paths for residual NMO+DMO for a series of depth points for offset 2 km, for $\gamma = 1.2$ and $\gamma = .833$. Like constant-offset residual-migration operators, the residual-NMO+DMO operators have cusps. Unlike residual constant-offset migration, the cusps occur at all combinations of depth and offset (except zero-offset). Also unlike residual constant-offset migration, eventually residual NMO+DMO shrinks to a point as depth increases and offset is fixed; the residual-NMO+DMO operator becomes equivalent to a residual-NMO operator.

Amplitudes of residual-NMO+DMO operators are obtained with the same method used to obtain the amplitudes of constant-offset residual-migration operators. Compute the discrete operator for an output point in equal increments of the original integration variables and use the formulae from Appendix B section 2 to get the summation weights. When the operator is spatially aliased, recompute the points on the summation path

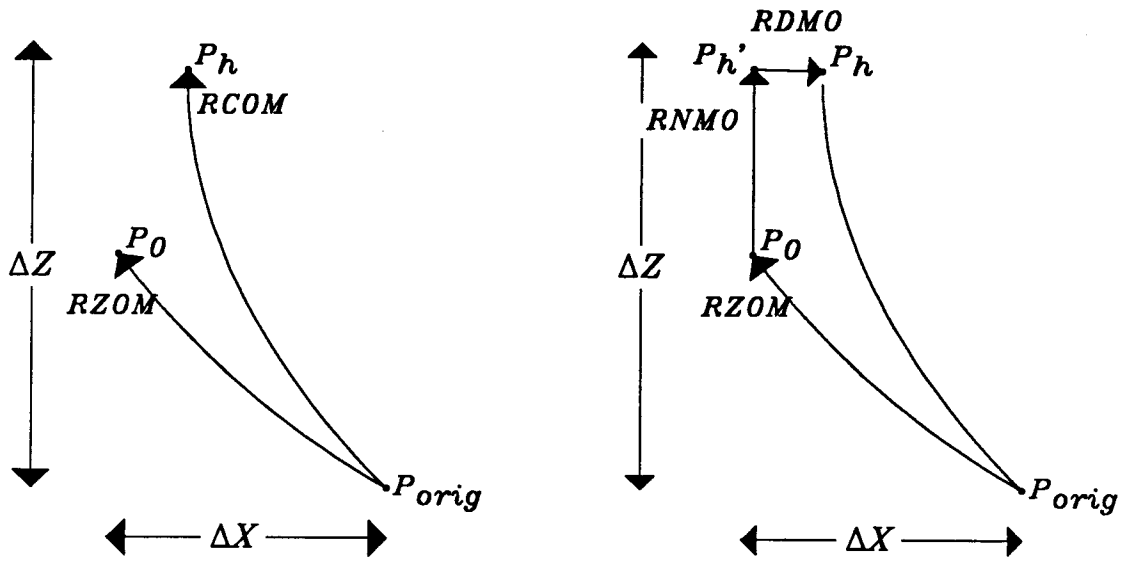

FIG. 2.7. Decomposing residual constant-offset migration (RCOM) into residual zero-offset migration (RZOM), residual normal moveout (RNMO), and residual dip moveout (RDMO).

in equal arc length and multiply by the Jacobian of the change in variables (computed numerically). When the operator shrinks to less than the discretization of the input image, interpolate the operator onto the input grid with a sinc interpolator or replace residual NMO+DMO with residual NMO.

If the cost of residual NMO+DMO, which is less than the cost of residual constant-offset migration, is still too high for a particular application, it is possible to use only residual NMO. Interpreting Figure 2.8, the greatest error of this approximation is for large offset/depth ratios which are often muted anyway.

2.3.4 Velocity analysis

The lack of moveout over offset of an event is an indication that the interval-velocity model used for prestack depth migration of the constant-offset sections correctly predicts the differences in traveltime over offset of the reflected waves that describe the event. The presence of residual moveout means that the velocity model used for migration does not model the traveltimes of the reflected waves for different offsets, indicating an error in the part of the velocity model that affects the reflector (Al-Yahya, 1989).

Residual prestack migration and especially residual NMO+DMO can perform velocity analysis after an initial prestack migration. Inspired by conventional velocity estimation and section 1.3, I apply residual NMO+DMO to depth-migrated constant-offset sections for a range of residual velocities (in practice, use residual slowness). The residual velocity that best corrects the remaining moveout of an event after the initial migration is that event's residual velocity. Like DMO-corrected stacking velocities, residual velocities computed using residual NMO+DMO give structure-independent moveout estimates. Excluding the zero-offset residual-migration part of residual prestack migration avoids the problem of doing velocity analysis on moving events.

Also, like stacking velocity or migration velocity, residual velocity is an average or effective velocity and not an interval velocity itself. As long as the true residual moveout can be approximately described by residual time migration, residual-velocity estimates should be useful for interval-velocity analysis. Chapter 3 and Chapter 4 describe how to convert changes in interval velocity to residual velocity and vice versa.

2.4 Examples

Figure 2.9 shows a synthetic constant-offset section collected over a series of point diffractors and its migrated image using the correct velocity. The bottom of Figure 2.10 shows the constant-offset section migrated with an a slowness equal to .8333 times the correct slowness. The top of Figure 2.10 shows the result of applying residual constant-offset migration with $\gamma = 1.2$. The images of the point diffractors are successfully recovered. Figure 2.11 shows the result of applying residual NMO+DMO to the incorrectly migrated constant-offset section (bottom of Figure 2.10). After residual NMO+DMO, the image should differ from the true image by requiring only residual zero-offset migration. The top of Figure 2.11 shows the result of applying residual zero-offset migration after residual NMO+DMO. Again, the point-diffractor images are recovered. The small "glitch" in the image of the third point diffractor is an artifact of the switch from using the complete residual-NMO+DMO operator to just using residual NMO.

Residual constant-offset migration seems to focus the point diffractors better than residual NMO+DMO followed by residual zero-offset migration. There are two possible

reasons for this. First, building residual NMO+DMO uses more asymptotic approximations. Second, the residual-NMO+DMO operator has cusps for all depths, while the residual constant-offset migration operator only has cusps for large offset/depth ratios. The cusps correspond to higher-order stationary points whose contributions are more difficult to approximate accurately with the stationary phase method. Energy spreads away from these cusps rather than lying along a curvilinear trajectory. For evidence of this energy smearing, examine the overmigrated image of the upper point diffractor in Figure 2.10.

The presence of cusps only at large offset/depth ratios is one advantage of residual constant-offset migration over residual NMO+DMO followed by residual zero-offset migration. For small offset/depth ratios, the cusps do not cause difficulties for residual NMO+DMO however, because the operator effectively reduces to a point operator (more accurately, a dip-limited delta-function), namely residual NMO. The fact that the size of the residual-NMO+DMO operator shrinks with depth gives it an advantage in computational cost over residual constant-offset migration.

Figure 2.12 shows one constant-offset section taken at an offset one-half the total cable length of a seismic survey in the Gulf of Mexico. All constant-offset sections from the survey were depth-migrated with a velocity model that was a function of depth only and purposely chosen to undermigrate the data. After prestack migration, I binned and stacked together every 12 migrated constant-offset sections to increase the signal-to-noise ratio, remove artifacts, and reduce the data volume. Figure 2.13 shows one partial stack of migrated constant-offset sections.

After migration and partial stacking, residual NMO+DMO was applied to the migrated constant-offset sections for residual slowness in the range $0.645 < \gamma < 1.15$. Figures 2.14, 2.15, and 2.16 show the stack of all constant-offset sections after residual NMO+DMO with different values of γ. At the lower values of γ, corresponding to the largest increase in velocity, the deeper events stack well. At the higher values of γ, closer to the original velocity, the shallower events stack well. Note that events stay fixed as their residual slowness γ changes. It is easier to find residual velocities using residual NMO+DMO than by scanning migration velocity with many full prestack migrations that force events to move as the migration slowness changes.

To see the reflectors at their residual time-migrated locations, apply residual zero-offset migration to the stacks of Figures 2.14–2.16. Figures 2.17–2.19 show the result of residual zero-offset migration applied to each stack at its appropriate value of γ. These panels

illustrate a different kind of velocity information. Figures 2.14–2.16 give velocity cues based only on stack coherency; Figures 2.17–2.19 give velocity cues based primarily on structural information. This latter kind of velocity information, geological reasonability, is powerful velocity information to an interpreter but difficult to automate with a computer.

Figure 2.20 shows sample panels of residual slowness versus semblance extracted from the velocity-analysis cube. This velocity analysis is a residual time-migration velocity analysis after prestack depth migration. From these panels one can pick the residual prestack time migration that best corrects the moveout of an event that remains after prestack depth migration. This type of velocity analysis has the robust properties of conventional velocity analysis discussed in Chapter 1.

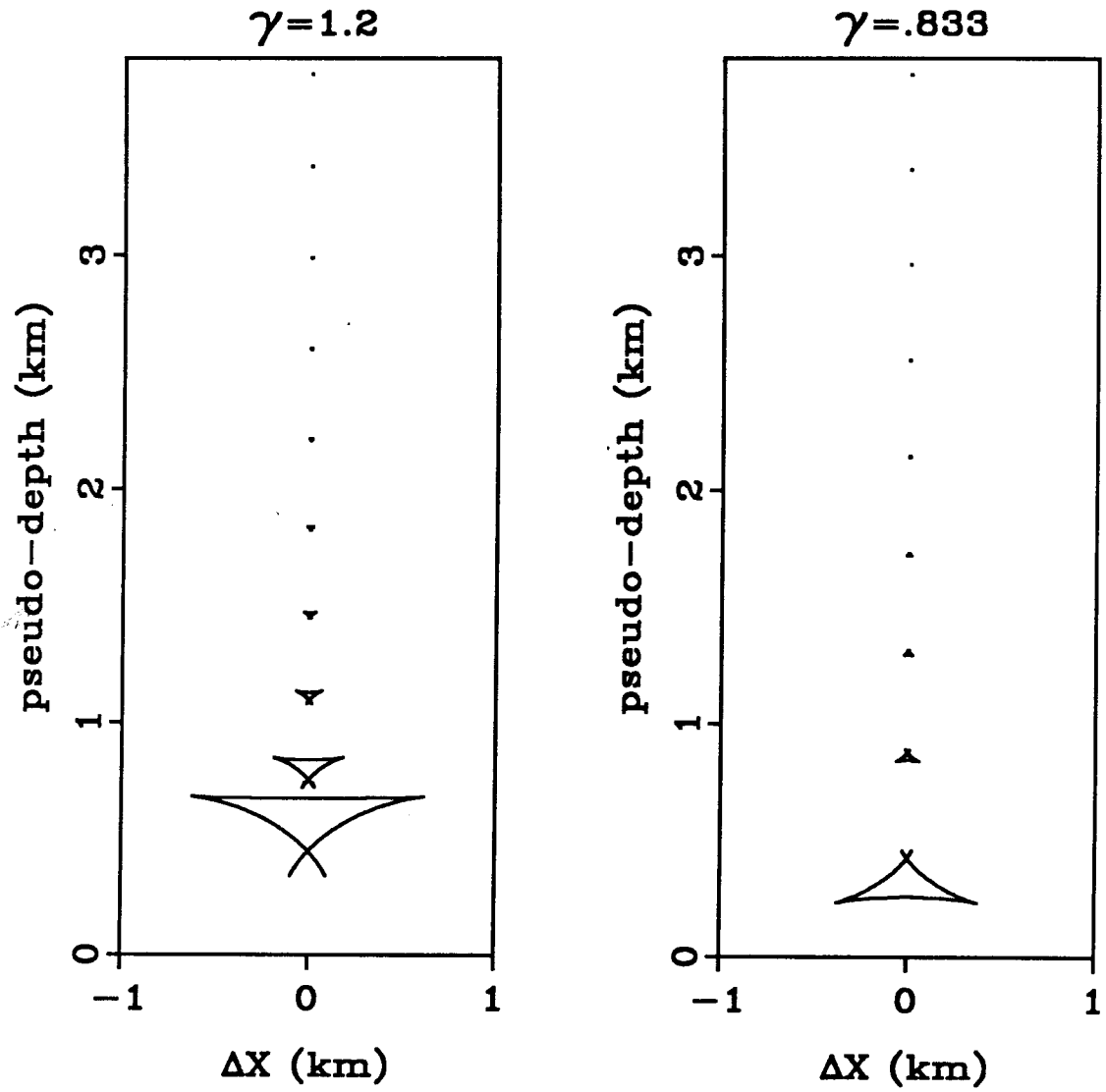

FIG. 2.8. Integration paths for residual NMO+DMO for a series of depth points; offset=1 km. Residual slowness for the left plot: $\gamma = 1.2$. Residual slowness for the right plot: γ=.8.

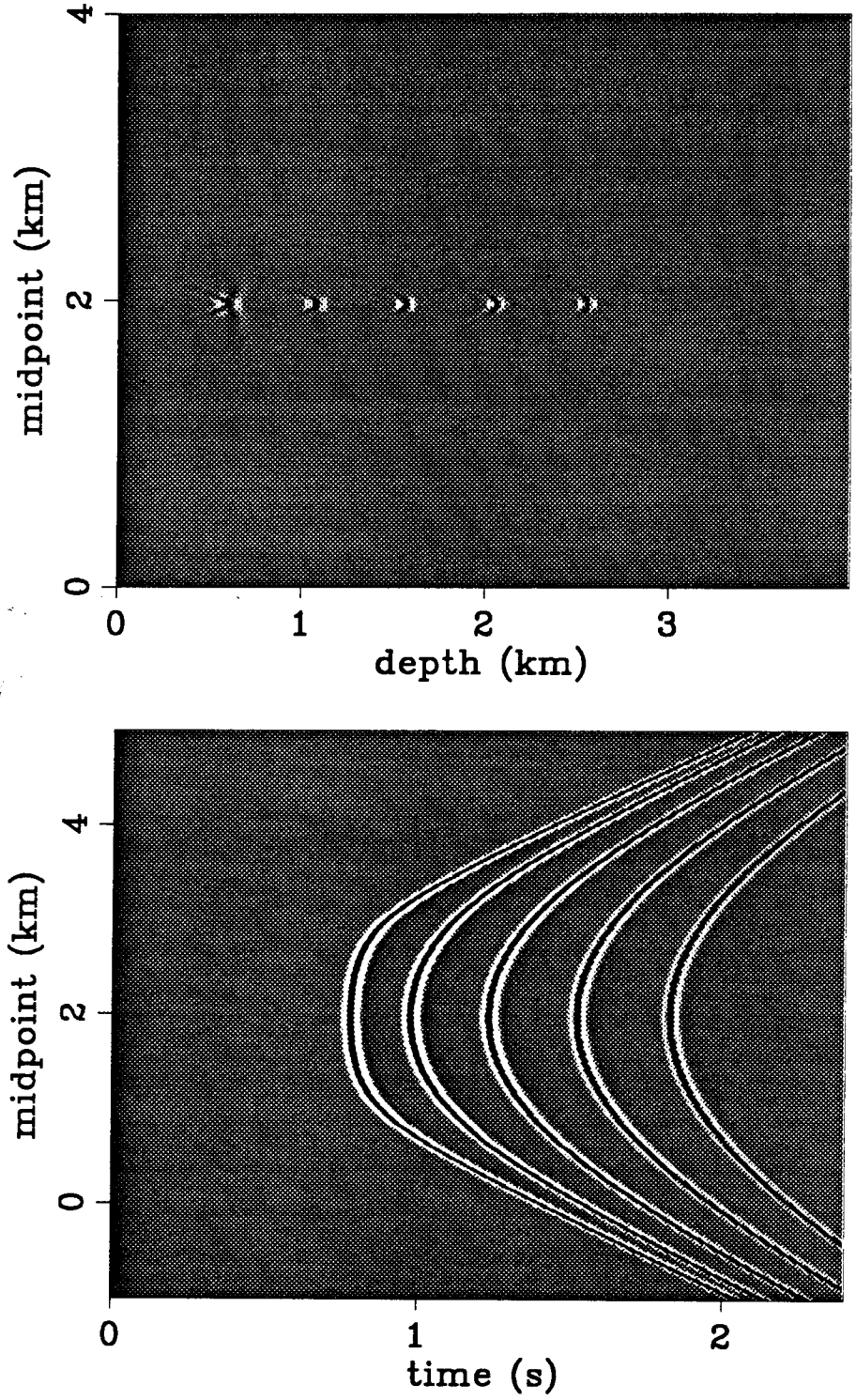

FIG. 2.9. The lower plot shows constant-offset data collected in constant velocity over a series of point diffractors. The upper plot shows the correctly migrated image of the point diffractors.

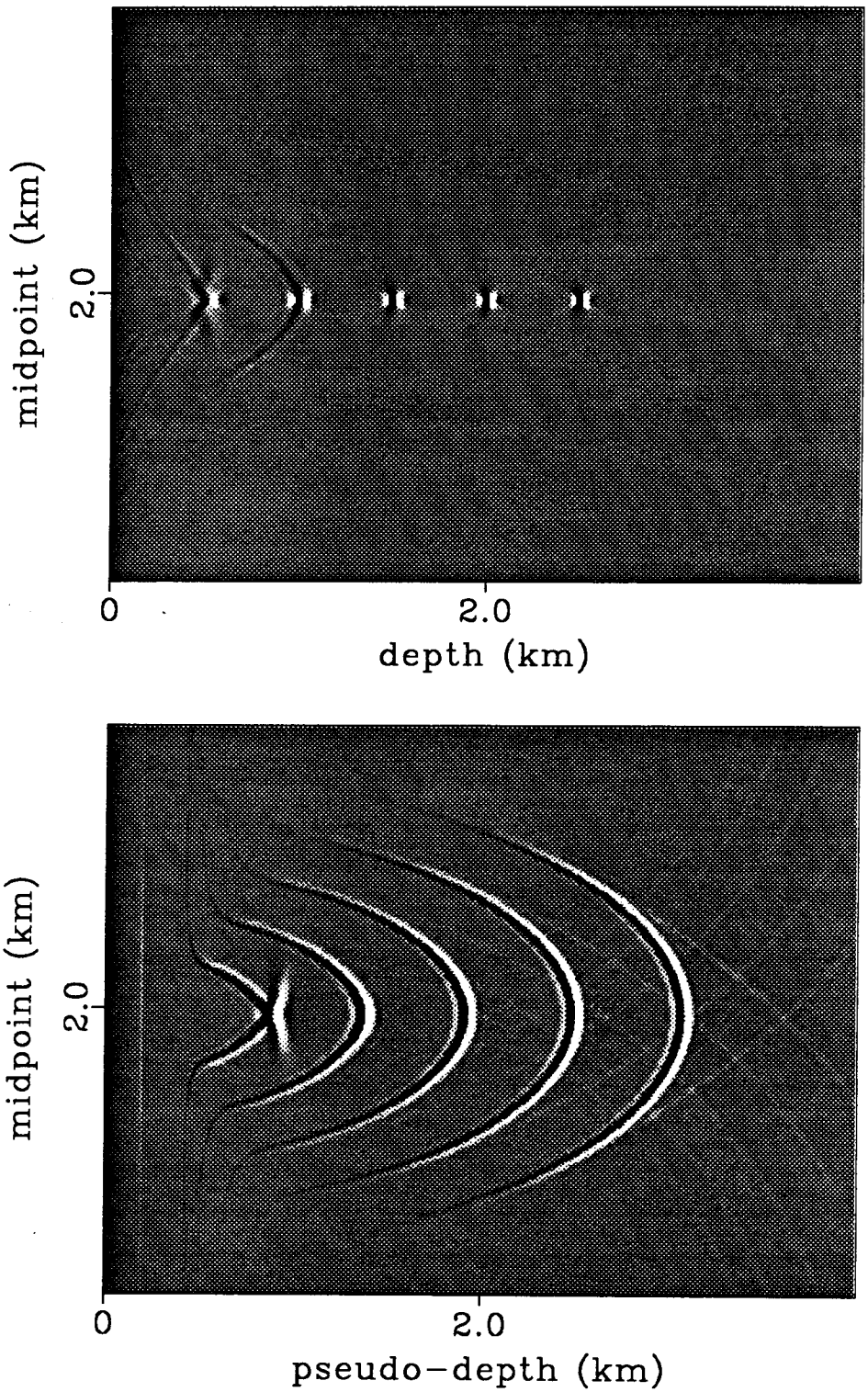

FIG. 2.10. Point-diffractor model. The lower plot is a migrated constant-offset section, migrated with a slowness equal to .8333 times the correct slowness. The upper plot shows the result of applying residual constant-offset migration at $\gamma = 1/.8333 = 1.2$ to recover the image of the point diffractors.

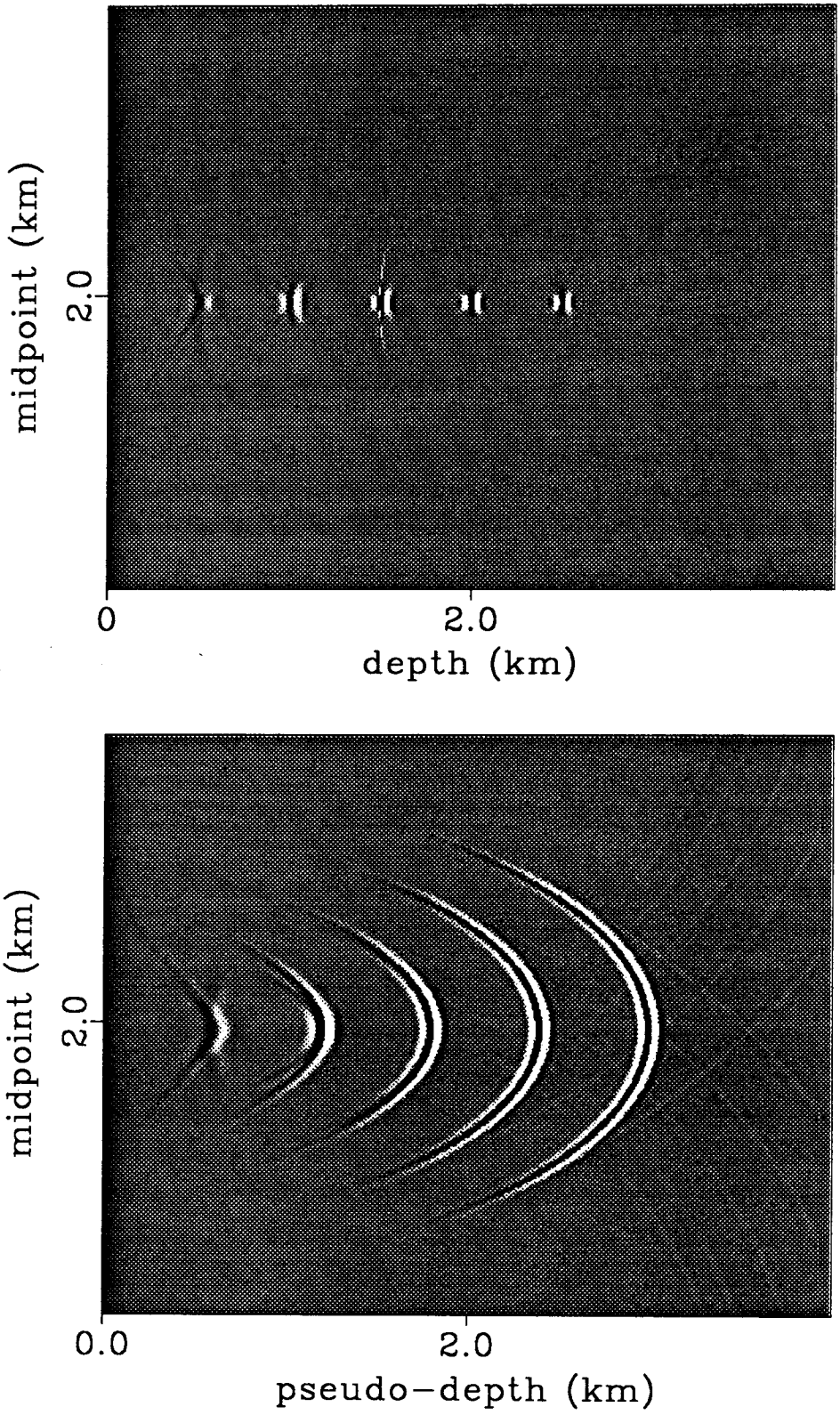

FIG. 2.11. Point-diffractor model. The lower plot is the migrated constant-offset section of Figure 2.9 after residual NMO+DMO applied with $\gamma = 1.2$. The upper plot shows the result of applying residual zero-offset migration at $\gamma = 1.2$ after residual NMO+DMO to recover the image of the point diffractors.

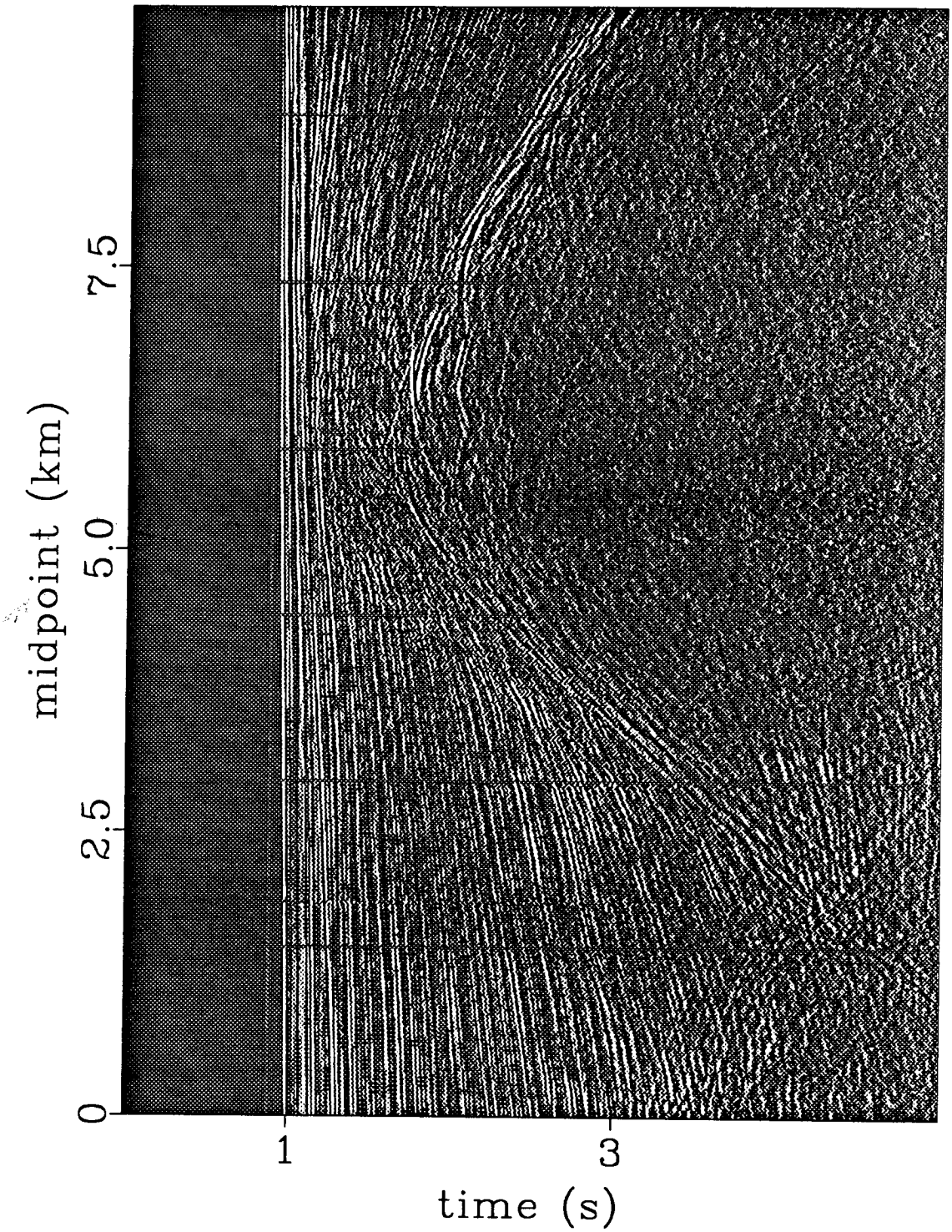

FIG. 2.12. A constant-offset section from a Gulf of Mexico data set used as input to constant-offset prestack migration.

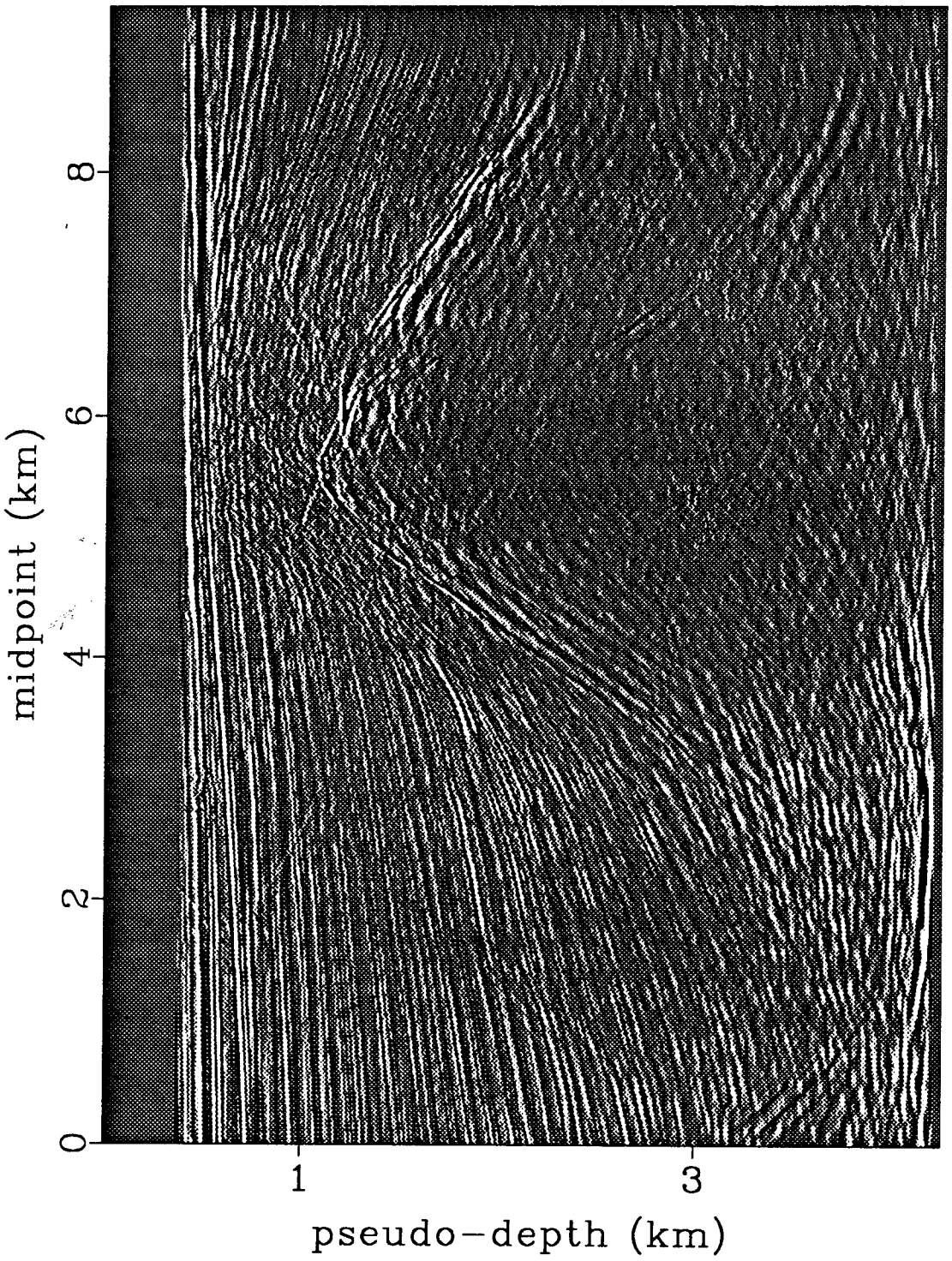

FIG. 2.13. Partial stack of 12 migrated nearby constant-offset sections. The interval-velocity model was purposely chosen to undermigrate the data (velocities too slow).

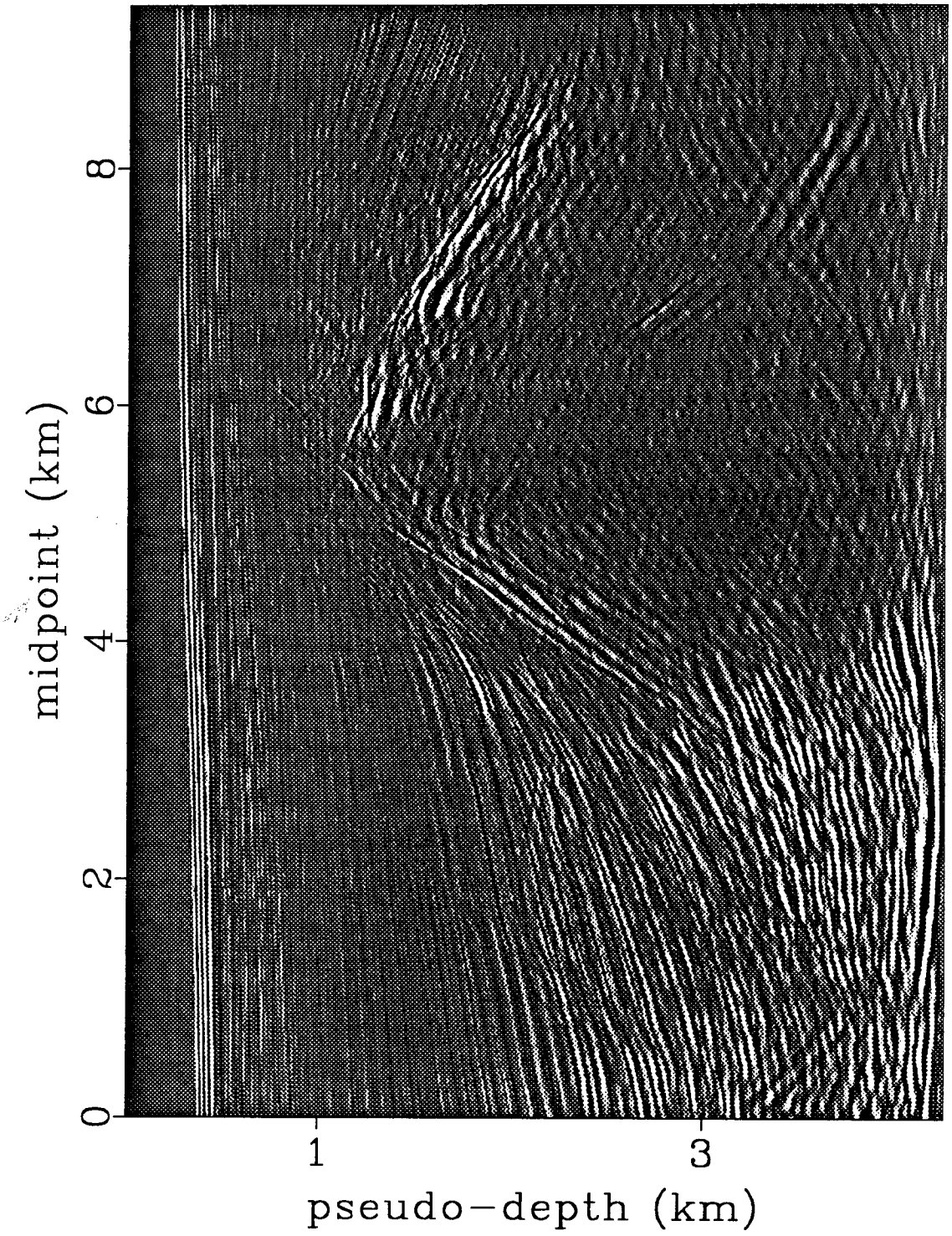

FIG. 2.14. Stacked section after prestack migration and residual NMO+DMO using $\gamma = .745$. Deeper events stack best because this γ corresponds to a large increase in the migration velocity.

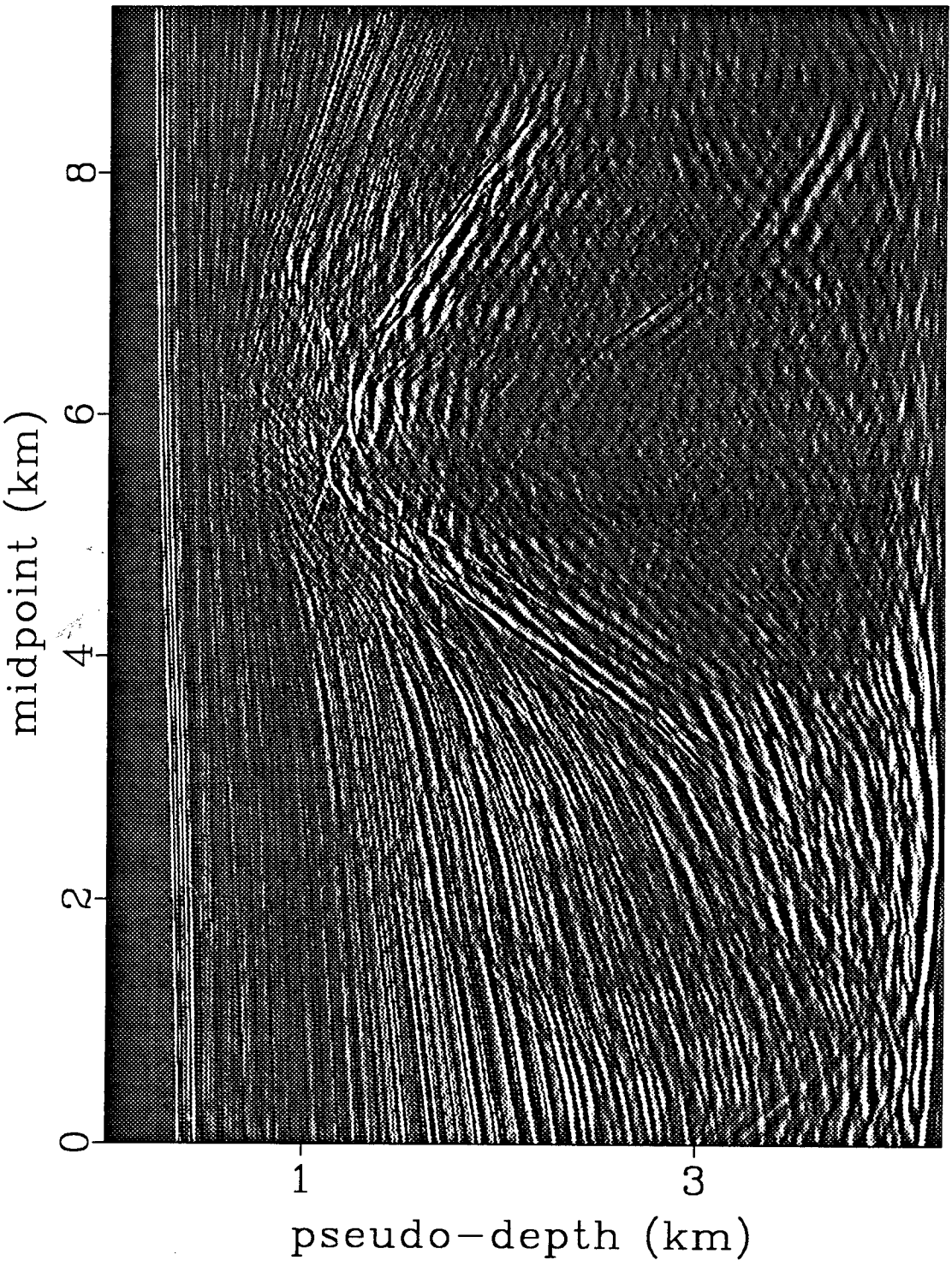

FIG. 2.15. Stacked section after prestack migration and residual NMO+DMO using $\gamma = .835$. Events in the middle of the section stack best corresponding to an intermediate increase in migration velocity.

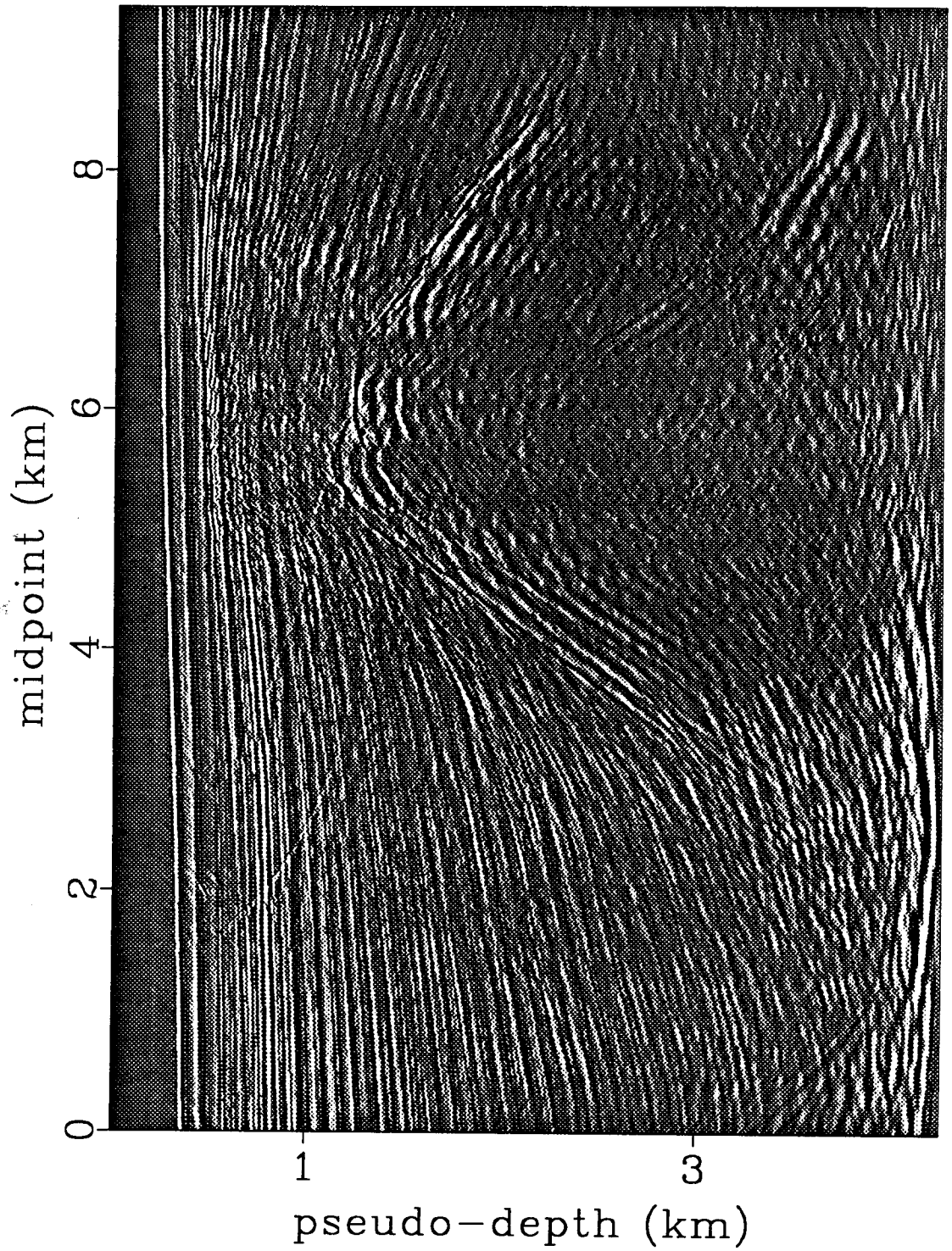

FIG. 2.16. Stacked section after prestack migration and residual NMO+DMO using $\gamma = .94$. Events near the water bottom stack best at this value of γ corresponding to only a small change in the migration velocity.

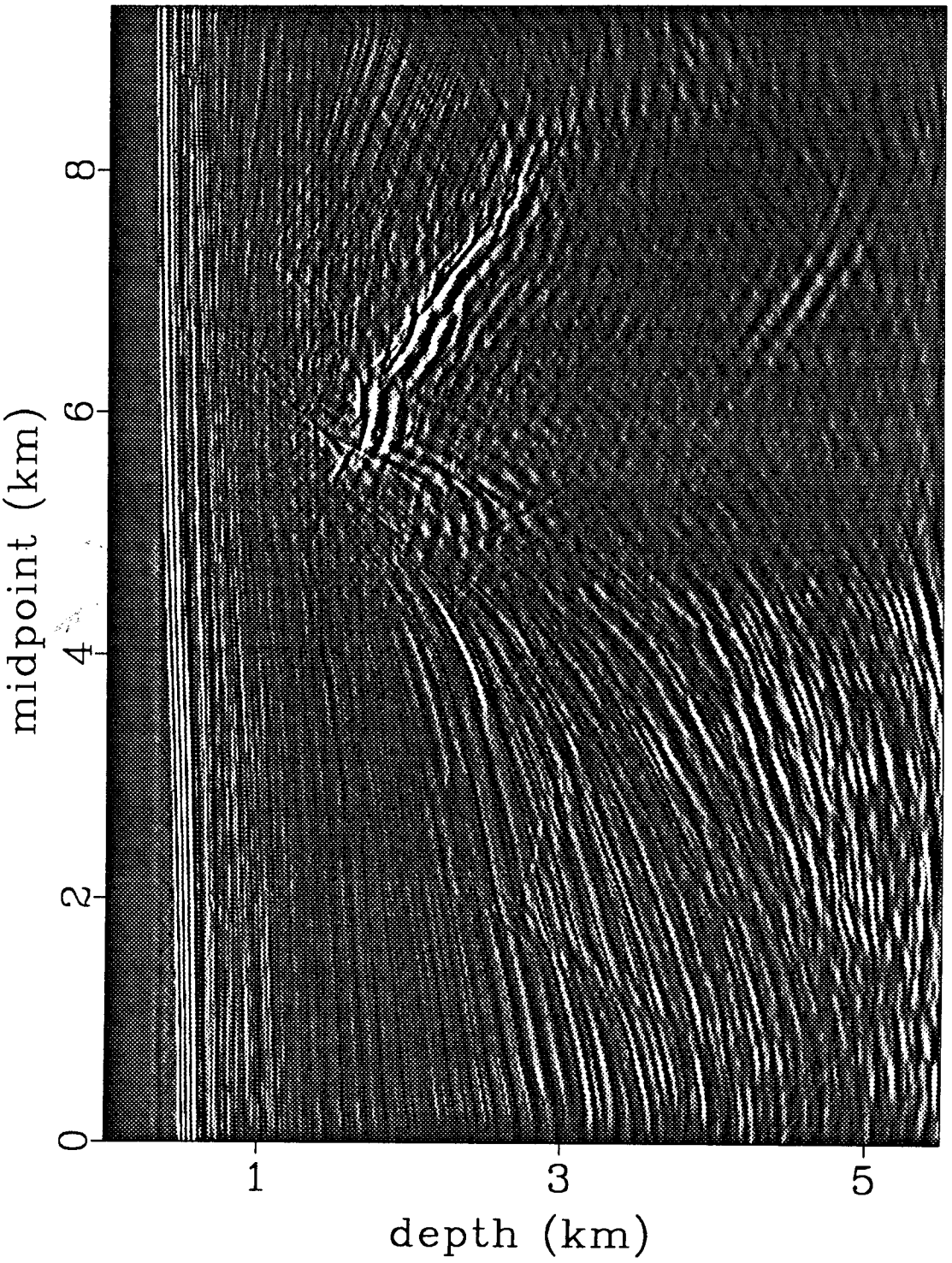

FIG. 2.17. Residual zero-offset migration applied at $\gamma = .745$ to the RNMO+DMO-corrected stack of Figure 2.12. Only the deepest part of the image is correctly migrated.

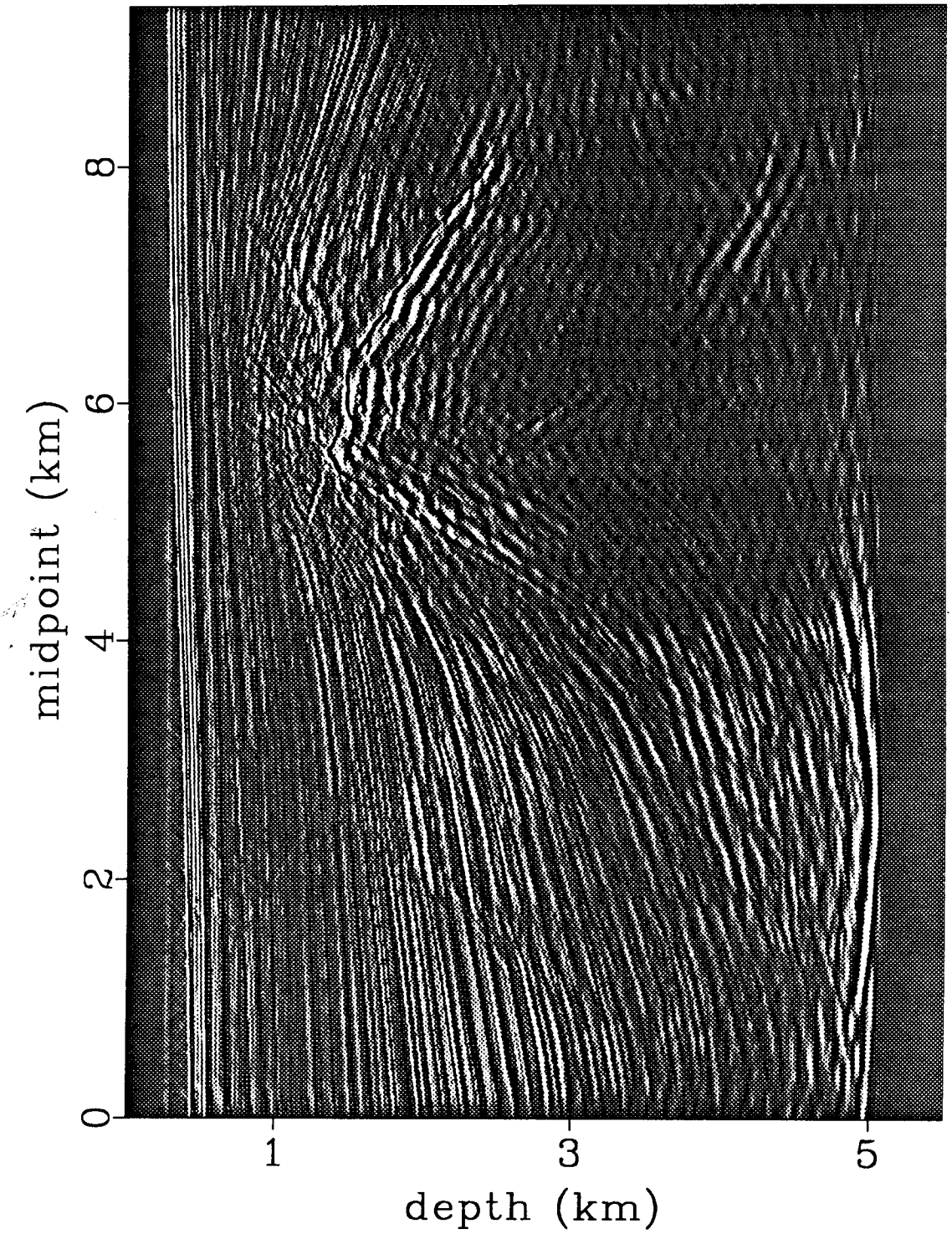

FIG. 2.18. Residual zero-offset migration applied at $\gamma = .835$ to the RNMO+DMO-corrected stack of Figure 2.13. The middle depths of the image are correctly migrated.

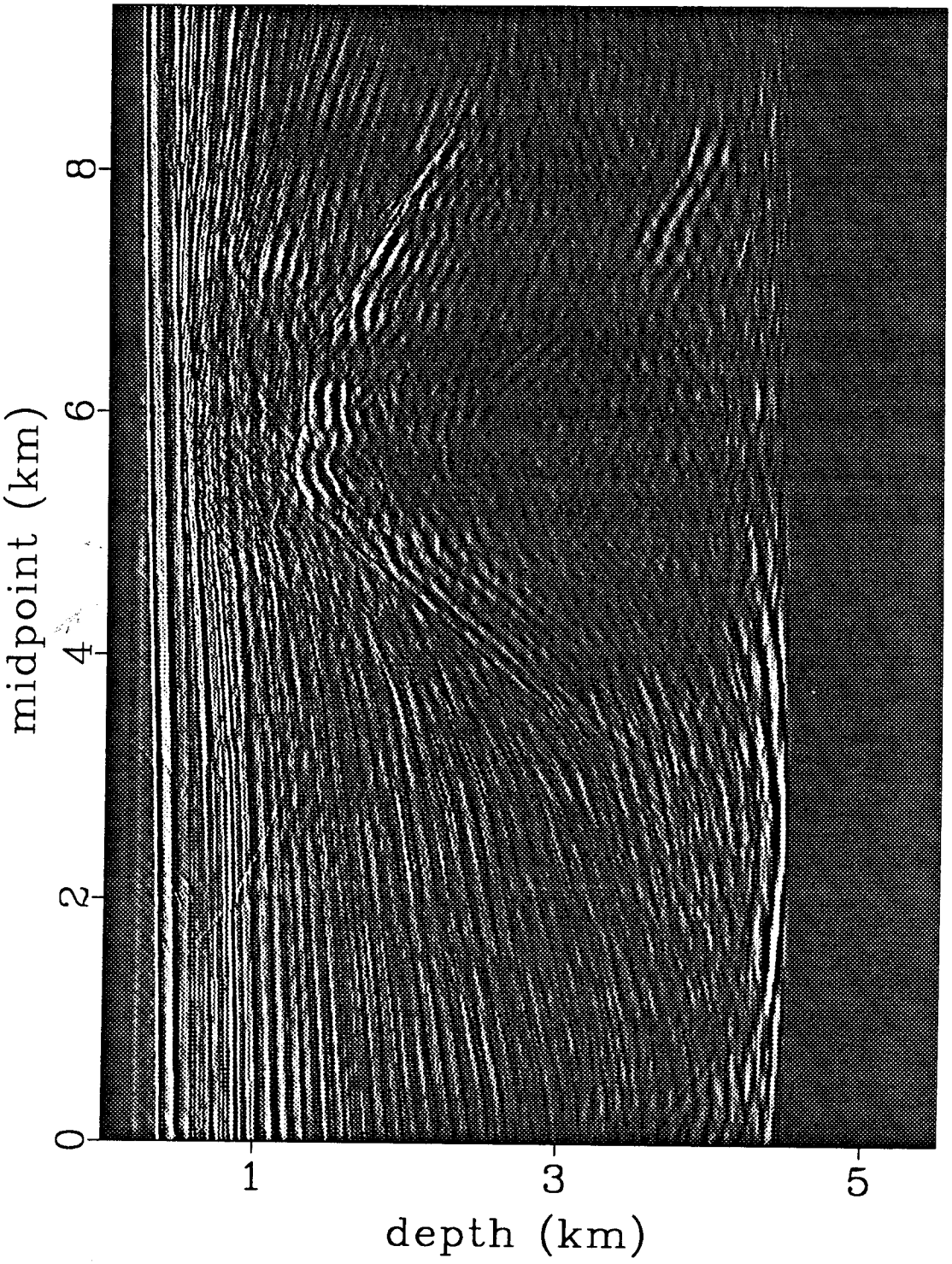

FIG. 2.19. Residual zero-offset migration applied at $\gamma = .94$ to the RNMO+DMO-corrected stack of Figure 2.14. The shallow reflectors are correctly migrated.

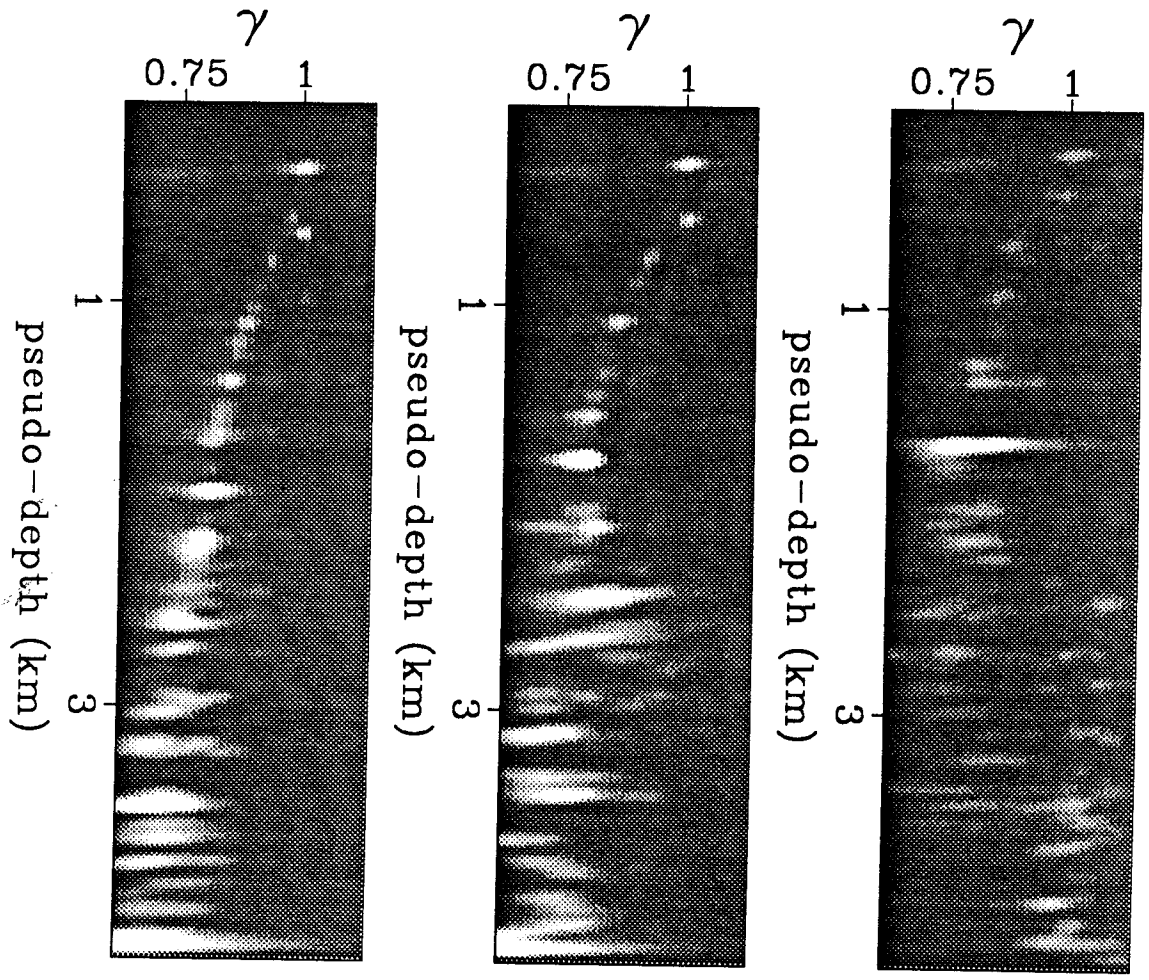

FIG. 2.20. Semblance spectra for 3 midpoints computed using RNMO+DMO. The peaks of the semblance tell how much residual prestack time migration should be applied to each event after the original prestack depth migration to correct residual moveout. The left panel comes from a midpoint to the left of the salt dome. The middle panel comes from the left flank of the salt dome. The right panel comes from the right flank of the salt dome.